ELSEVIER

Catalysis Today 77 (2002) 269–284

CATALYSIS TODAY

www.elsevier.com/locate/cattod

Synthesis and characteristics of MCM-41 supported CoRu catalysts

Joongjai Panpranot [a], James G. Goodwin Jr. [a,*], Abdelhamid Sayari [b]

[a] *Department of Chemical Engineering, Clemson University, Clemson, SC 29634, USA*

[b] *Centre for Catalysis Research and Innovation (CCRI), Department of Chemistry, University of Ottawa, Ottawa, Ont K1N 5N6, Canada*

Abstract

Supported CoRu catalysts have been prepared with ordered mesoporous silica (MCM-41) as the support using the incipient wetness impregnation method in order to study the effect of ordered mesoporous silica and pore size on cobalt dispersion, reduction behavior, and catalytic properties for the Fischer–Tropsch synthesis (FTS). Metal loadings of 2, 5, 8, and 14 wt.% Co with 0.5 wt.% Ru were investigated, as well as two different mesoporous silicas having average pore diameters of 3 and 7 nm. For comparison purposes, conventional amorphous silica (SiO_2) supported CoRu catalysts were also prepared using the same procedure. Due probably to higher concentration of water vapor in the small pores of MCM-41 during metal reduction, CoRu/MCM-41 catalysts showed stronger interaction of Co with the support than CoRu/SiO_2 as manifested by lower reducibilities of the catalysts during standard reduction. The Co dispersions were similar on MCM-41 to that on amorphous silica for a given Co loading. MCM-41 supported catalysts exhibited similar selectivities for FTS as to the SiO_2-supported ones; however, they had in general greater activities. There was an absence of any obvious pore size effect on product selectivity, probably due to the pores being sufficiently large for the reaction to easily proceed at 1 atm and 220 °C, the reaction conditions used. Thus, MCM-41 supported CoRu catalysts appear to be suitable for application to FTS. Their unique and tailored properties offer interesting possibilities for catalyst design and application in particular cases.

Keywords: MCM-41; Mesoporous silica; Cobalt catalysts; Ruthenium promotion; Fischer–Tropsch synthesis

1. Introduction

Cobalt-based catalysts are applied most widely for hydrogenation reactions in a variety of systems [1]. To increase the catalytic activity, cobalt is usually supported on a high surface area support in order to obtain a high metal dispersion. Various supports for cobalt have been used, including silica [2–7,39], alumina [2,8–11], kieselguhr [12], titania [2,13,14], magnesia [2], carbon [2,15], and zeolites [16,17]. Such catalysts exhibit a wide range of properties, such as specific surface area, cobalt dispersion, reduction behavior, and catalytic activity [18]. The presence of a small amount of a second transition metal such as Ru in addition to Co is known to increase the reducibility and dispersion of Co [10].

Highly ordered mesoporous silica, such as MCM-41, has been recently used as a support for metal catalysts, resulting in several cases in significant improvements when compared to conventional and commercial catalysts. For example, Corma et al. [19] have reported a superior hydrogenation activity and sulfur tolerance for Pt/MCM-41 catalysts compared

* Corresponding author. Tel.: +1-864-656-3056; fax: +1-864-656-0784.
E-mail address: james.goodwin@ces.clemson.edu (J.G. Goodwin Jr.).

0920-5861/02/$ – see front matter
PII: S0920-5861(02)00252-3

to Pt/zeolite-USY, Pt/SiO_2, and Pt/Al_2O_3. Song and Reddy [20] reported that Co–Mo supported on aluminosilicate MCM-41 catalysts prepared by impregnation showed higher hydrogenation and hydrocracking activities than conventional Co–Mo supported on γ-Al_2O_3 catalysts. In a more recent study by Schuth et al. [21], Fe_2O_3/MCM-41 was found to exhibit a superior performance for the conversion of SO_2 to SO_3 compared to Fe_2O_3 supported on conventional silica.

MCM-41 possesses high BET surface areas, uniform pore sizes with pore dimensions between 1.5 and 10 nm, and high thermal and hydrothermal stability. The better performances of MCM-41 supported catalysts have been attributed especially to their high surface areas and superior dispersion of the active metals.

In this study, MCM-41 was used as support for Ru-promoted Co catalysts suitable for the Fischer–Tropsch synthesis (FTS). Two kinds of pure silica (MCM-41) with different pore sizes were synthesized and employed. Our investigation focused on determining the effect of ordered mesoporous silica and its average pore size on cobalt dispersion, reduction behavior, and catalytic properties for the FTS. The results are compared to those for conventional amorphous silica-supported CoRu catalysts.

2. Experimental

2.1. Catalysts preparation

The pure silica (MCM-41) was prepared as reported elsewhere [22] using the following gel composition: (1.0 SiO_2):(0.33 TMAOaH):(0.17 NH_4OH):(17 H_2O), where TMAOH denotes tetramethylammonium hydroxide. Cab-O-Sil silica (40 g, from Cabot) was mixed manually with 67 g of water. Then, 68.2 g of 25% TMAOH aqueous solution (Aldrich) was added under vigorous magnetic stirring. Another mixture comprised of 40.5 g of CTMABr (Aldrich), 72 g of water, and 13 g of concentrated ammonia (BDH) was prepared during stirring, where CTMABr denotes cetyltrimethyl ammonium bromide. Both of these mixtures were transferred into a Teflon lined autoclave, stirred for 30 min, then heated statically at 70 °C for 3 days, then at 130 °C for 1 day. The obtained solid material was filtered, washed with water and dried at 60 °C. The sample was then calcined in flowing nitrogen up to 550 °C (1–2 °C/min), then in air at the same temperature for 5 h, and is referred to in this paper as small pore MCM-41 or M1. The larger pore MCM-41 or M2 was prepared by treating the small pore MCM-41 (prior to calcination) in an emulsion containing *N*,*N*-dimethyldecylamine (0.625 g in 37.5 g of water for each gram of MCM-41). The treatment was carried out for 3 days at 120 °C. The obtained samples were washed thoroughly, dried, and calcined in flowing nitrogen up to 550 °C (1–2 °C/min), then in air at the same temperature for 5 h. For comparison purposes, conventional amorphous silica (Davison silica grade 952) was also used as a catalyst support.

The series of supported CoRu catalysts (2–14 wt.% Co and 0.5 wt.% Ru) were prepared by the incipient wetness impregnation of the supports (M1, M2, and amorphous silica) with an aqueous solution containing the desired amount of cobalt nitrate (J.T. Baker) and ruthenium nitrosyl nitrate (STREM Chemicals). The catalysts were dried overnight in an oven at 120 °C and calcined at 300 °C in an air flow for 2 h. CoRu catalysts supported on the small pore MCM-41 catalysts are referred to as 2CoRu/M1, 5CoRu/M1, 8CoRu/M1, and 14CoRu/M1, where the initial number denotes the wt.% of Co. CoRu catalysts supported on the large pore MCM-41 are referred to as 2CoRu/M2, 5CoRu/M2, 8CoRu/M2, and 14CoRu/M2. CoRu catalysts supported on amorphous silica (SiO_2) catalysts are referred to as 2CoRu/S, 5CoRu/S, 8CoRu/S, and 14CoRu/S. The final Co loadings of the catalysts were determined using inductively coupled plasma (ICP) spectroscopy (Galbraith Laboratories).

2.2. BET surface area and pore size distribution

The BET surface area, pore volume, average pore diameter, and pore size distribution of the catalysts were determined by N_2 physisorption using a Micromeritics ASAP 2010 automated system. Each sample was degassed in the Micromeritics ASAP 2010 at 200 °C for 4 h prior to N_2 physisorption.

2.3. X-ray diffraction

A Scintag 2000 X-ray diffractometer with monochromatized Cu Kα radiation (40 kV, 40 mA) and a Ge detector was used for the XRD measurements. The spectra were scanned with a rate of 0.5 °/min from

1.5° to 7.0° 2θ and with a rate of 3 °/min from 20° to 70° 2θ. The cobalt and ruthenium phase were identified by comparison with the JCPDS database and average crystallite sizes (d_p) were calculated using the Scherrer equation [23].

2.4. Temperature programmed reduction

The reducibilities of the calcined cobalt catalysts were measured by temperature programmed reduction (TPR) using an Altamira AMI-1 system. TPR used a temperature ramp of 5 °C/min from 30 to 800 °C in a flow of 5% H_2 in Ar. H_2 consumption was measured by analyzing the effluent gas with a thermal conductivity detector. The detector output was calibrated by reduction of Ag_2O powder.

2.5. Hydrogen chemisorption

Percent metal dispersion and average Co particle size of the reduced catalysts were calculated based on the results from H_2 chemisorption. H_2 chemisorption was carried out following the procedure described by Reuel and Bartholomew [2] using a Micromeritics chemisorption ASAP 2010 automated system. Prior to chemisorption, the catalysts were evacuated at 100 °C for 15 min, reduced at 100 °C for 15 min, reduced at 350 °C for 10 h after ramping up to a rate of 1 °C/min, and desorbed at 350 °C for 90 min at 10^{-6} mm Hg. The number of exposed metal atoms on the surface was calculated by extrapolating the total adsorption isotherm to zero pressure and assuming coverage of one H atom per Co^0 atom exposed on the surface.

2.6. Scanning electron microscopy

Catalyst granule morphology and elemental distribution were obtained using a Hitachi S-3500N scanning electron microscopy (SEM). The SEM was operated using the back scattering electron (BSE) mode at 20 kV and a working distance (the distance between the sample and the electron beam) of 15 mm. After the SEM micrographs were taken, EDX was performed to determine the elemental concentration distribution on the catalyst granules using INCA software.

2.7. Reaction

FTS was performed in a down-flow differential fixed-bed stainless steel reactor at atmospheric pressure and 220 °C. A GHSV of ca. 20,000 h^{-1} and a H_2/CO ratio of 2 were used. The reaction temperature was controlled by a thermocouple inserted into the catalyst bed. A catalyst (ca. 200 mg) was held in the middle of the reactor using quartz wool. It was first heated in 50 cc/min H_2 flow to 350 °C, using a ramp rate of 1 °C/min, and then reduced in situ at this temperature for 10 h prior to reaction. In order to avoid exotherms and hot spots that lead to rapid catalyst deactivation, the reaction was initiated in a controlled manner by gradually increasing the reactant concentrations over a period of 2 h. After the start-up, samples were taken at 3 h intervals and analyzed by GC (Varian CP-3800). Reaction was continued at 220 °C for 24 h in order to determine time-on-stream behavior to steady-state reaction.

3. Results

3.1. N_2 physisorption

BET surface areas, pore volumes, and average pore diameters of the catalysts are given in Table 1. SiO_2-supported catalysts had BET surface areas between 200 and 300 m^2/g and large pore volumes. The BET surface areas of the catalysts supported on mesoporous silica (M1 or M2) were significantly higher (600–1100 m^2/g) in the order of CoRu/M1 > CoRu/M2 > CoRu/SiO_2 for a given loading of Co, reflecting the significant difference in surface areas of the original support materials. The BET surface area and pore volume of the catalysts decreased with Co loading, the decrease however being more significant in the case of M1-supported CoRu catalysts. For the maximum Co loading of 14 wt.%, BET surface area of the supports decreased by ca. 50, 30, and 25% for M1, M2, and SiO_2, respectively. The pore size distributions of M1- and M2-supported CoRu catalysts are shown in Figs. 1 and 2, respectively. Both series of supported CoRu catalysts had narrow pore size distributions. The average pore diameters for the small (M1) and the large (M2) pore MCM-41 were determined to be approximately 3 and 7 nm, respectively. Co loading did

Table 1
N_2 physisorption results

Catalysts	BET surface area (m^2/g)[a]	Pore volume (cm^3/g)[b]	Average pore diameter (nm)[b]
SiO_2	293	1.78	23.7
2CoRu/S	285	1.57	22.0
5CoRu/S	264	1.49	22.6
8CoRu/S	262	1.48	22.5
10CoRu/S	219	1.23	22.6
M1	1226	0.85	2.8
2CoRu/M1	1087	0.67	2.5
5CoRu/M1	987	0.60	2.4
8CoRu/M1	726	0.39	2.1
14CoRu/M1	650	0.34	2.1
M2	901	1.59	7.0
2CoRu/M2	885	0.98	4.4
5CoRu/M2	790	0.71	3.6
8CoRu/M2	687	0.63	3.7
14CoRu/M2	610	0.62	4.1

[a] Error of measurement was ±10%.
[b] Error of measurement was ±5%.

not appreciably change the average pore diameter of the SiO_2. It did however decrease that of M1 and M2.

3.2. X-ray diffraction

The X-ray diffraction (XRD) patterns of the two kinds of mesoporous silica (M1 and M2) are displayed in Figs. 3 and 4, respectively. Only M1 exhibited the highly distinct pattern at low 2θ angles reflecting the ordered structure of MCM-41. M2 showed only a broad peak in the XRD pattern at higher 2θ angles (ca. 23.7°), similar to that of amorphous silica. Diffraction peaks at 2θ angles below 1.5° could not be measured accurately because of instrumentational reasons. Effect of Co loading on XRD patterns at low 2θ angles of the M1-supported CoRu catalysts is shown in Fig. 5.

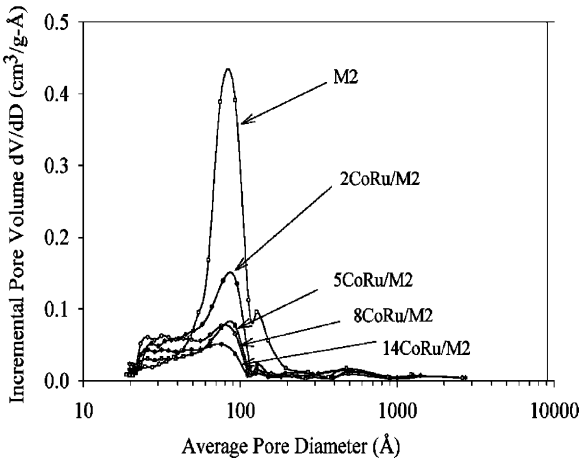

Fig. 2. Pore size distribution of M2 and M2-supported CoRu catalysts.

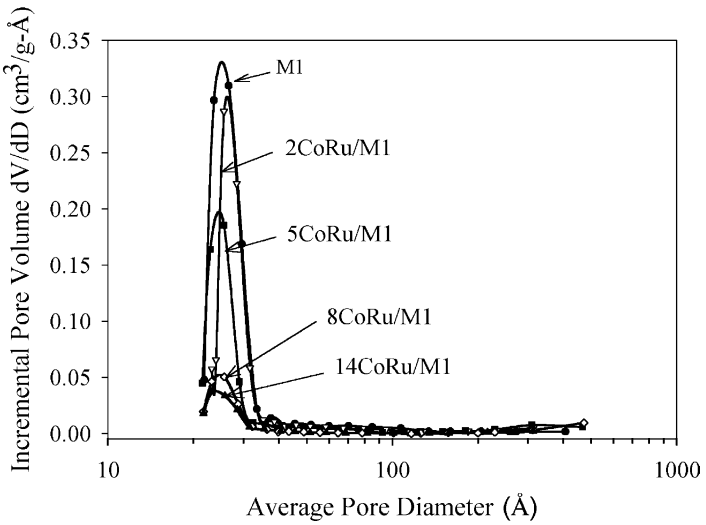

Fig. 1. Pore size distribution of M1 and M1-supported CoRu catalysts.

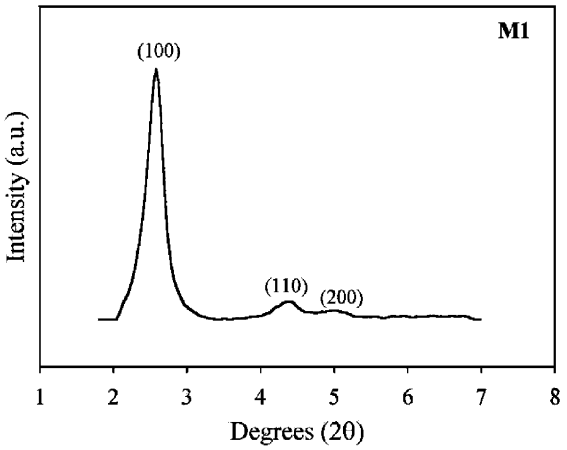

Fig. 3. XRD pattern for M1.

After impregnation of Co and Ru, the XRD pattern for MCM-41 diminished and disappeared for catalysts with Co loadings $\geq$ 5 wt.%. However, after removal of the metals by acid leaching of the 5CoRu/M1 catalyst, the XRD characteristic peak of MCM-41 was again detectable (Fig. 6), suggesting that the structure of MCM-41 was not destroyed by preparation of the CoRu catalysts as also suggested by the retention of the same average pore diameter ca. 3 nm.

During XRD, Co thus acted as an X-ray scatterer. The XRD patterns at higher diffraction angles of the calcined SiO_2-, M1-, and M2-supported CoRu catalysts are shown in Fig. 7. The diffraction peaks at 2θ of ca. 31.3°, 36.8°, 45.1°, 59.4°, and 65.4° indicate that after calcination at 300 °C, cobalt was primarily in the form of Co_3O_4 spinel on all the catalysts. The higher is the cobalt content, the stronger is the XRD intensity of the cobalt oxide became for all three types of supported CoRu catalysts. For the lowest Co loading (2 wt.% Co), XRD peaks due to ruthenium oxide (RuO_2) were also observable at 2θ of ca. 28.0°, 35.1°, and 54.3° on all the catalysts. For catalysts with higher Co loadings, the XRD peaks for RuO_2 were not observable because of the relatively small amount of ruthenium in the catalysts compared to cobalt. The average crystallite sizes of Co_3O_4 (d_0) in the original calcined catalysts were calculated using X-ray line broadening (Table 2). Co_3O_4 has to be reduced to cobalt metal (Co^0) prior to reaction since cobalt metal is known to be the most active phase for CO hydrogenation, not its oxides [24]. However, Co metal was not detectable by XRD for the reduced catalysts (not shown here) probably due to its particle sizes being near or below the lower limit for the XRD detectability (5 nm), as supported by the H_2 chemisorption results (Table 2).

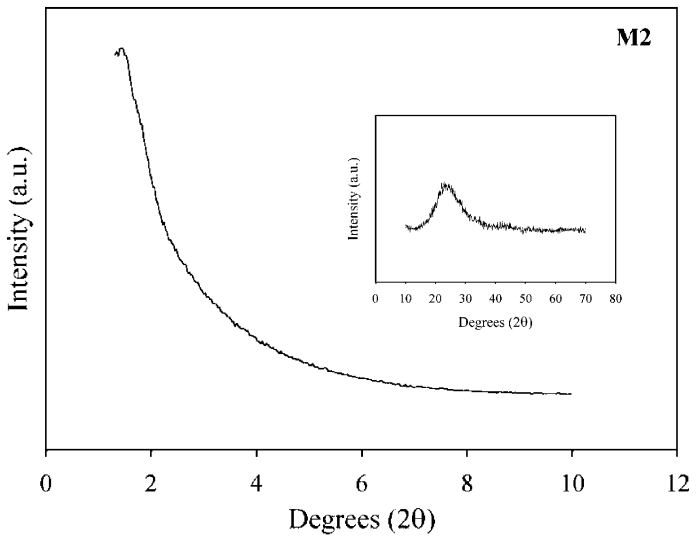

Fig. 4. XRD pattern for M2.

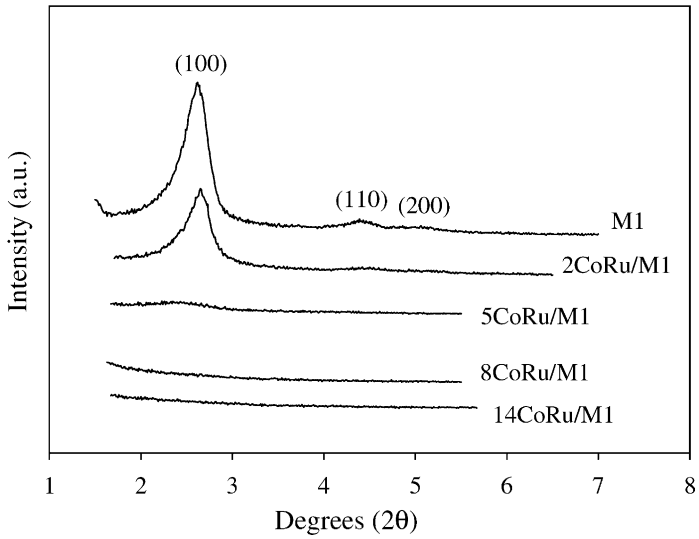

Fig. 5. Effect of cobalt loading on the XRD pattern of M1.

3.3. Temperature programmed reduction

TPR profiles of the SiO_2-, M1-, and M2-supported CoRu catalysts are shown in Figs. 8–10, respectively. The TPR profile of bulk Co_3O_4 is also given in Fig. 8. The reduction peak for bulk Co_3O_4 can be assigned to the two-step reduction of Co_3O_4 to CoO and then to Co^0 [25,26]. The SiO_2-supported CoRu catalysts exhibited two major reduction peaks. In general, TPR profiles are more complex for supported Co catalysts than for bulk Co_3O_4 due to various causes such

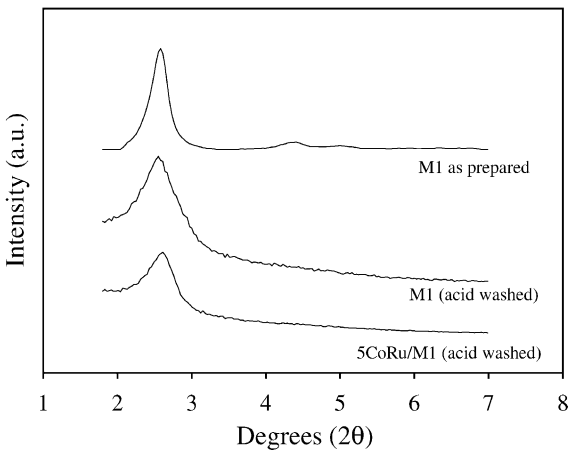

Fig. 6. XRD results for acid-leached 5CoRu/M1.

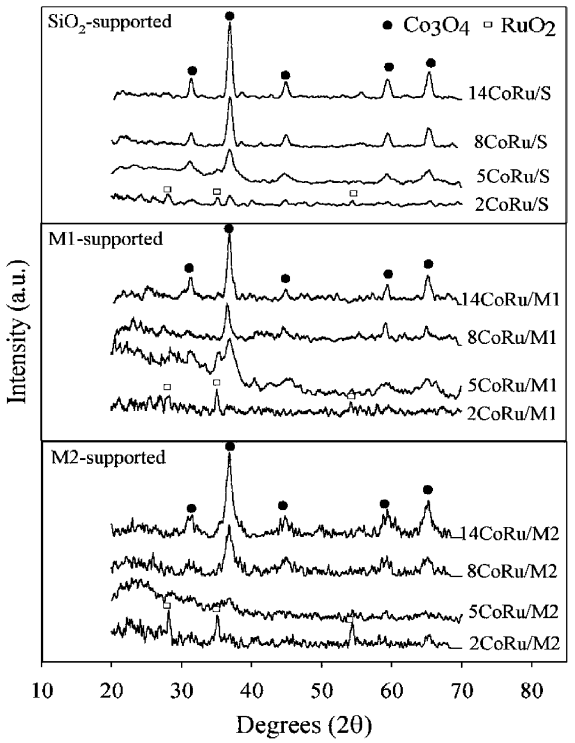

Fig. 7. XRD results for the calcined SiO_2-, M1-, and M2-supported CoRu catalysts.

Table 2
Characterization results

Catalyst	Co (wt.%)	% Reduction[a]		H_2 chemisorption[a]			XRD[b], Co_3O_4, d_o (nm)
		During TPR 30–800 °C	During TPR 30–400 °C[c]	Total[d] (μmol H_2/g cat.)	Average d_r[e] of Co^0 (nm)	% Co dispersion[f]	
2CoRu/S	1.9	68	68	21.4	4.9	13.2	–
5CoRu/S	4.3	68	68	35.7	6.7	9.8	–
8CoRu/S	8.3	65	65	64.7	6.8	9.2	13
14CoRu/S	14.2	70	58	92.6	7.2	7.7	16
2CoRu/M1	1.8	62	59	21.9	3.9	14.6	–
5CoRu/M1	4.6	63	57	49.1	4.3	12.7	–
8CoRu/M1	7.8	65	39	54.5	4.5	8.3	16
14CoRu/M1	14.4	69	38	58.7	7.6	4.8	23
2CoRu/M2	1.8	60	60	20.9	4.3	13.6	–
5CoRu/M2	4.2	64	58	42.4	4.6	12.0	–
8CoRu/M2	7.6	65	49	54.9	5.5	8.6	13
14CoRu/M2	14.2	70	47	116.1	4.7	9.7	15

[a] Error of measurements was ±5%.
[b] Based on XRD results of the calcined catalysts.
[c] Correlates to percentage of metal reduced during standard reduction procedure (ramp 1 °C/min to 350 °C, hold for 10 h).
[d] Extrapolated to zero pressure.
[e] Based on the reduced cobalt during standard reduction (used TPR 30–400 °C data), assuming $H/Co_s = 1$ and $d_r = 5$/(metal surface area)/(g reduced Co)/(Co density).
[f] Based on the total cobalt.

as variation in metal particle size on the support, metal–support interaction, and influence of support porous structure resulting in differently reducible cobalt species on the support [27–30]. A peak due to the decomposition of any $Co(NO_3)_2$ remaining after calcination is not likely to be present in this case since it has been reported that for Co/SiO_2, residual nitrate remains only when the catalyst precursors starting from cobalt nitrate have been calcined below 250–300 °C [31]. Calcination temperatures of 300 °C or higher for Co/SiO_2 catalysts result in the nitrate being completely thermally decomposed [29]. Many researchers have concluded that the two major reduction peaks in the TPR profiles of Co/SiO_2 or $CoRu/SiO_2$ can be assigned to two different species of Co_3O_4 [3–5,27–30]. The first peak located at ca. 135–230 °C is assigned to the reduction of large Co_3O_4 particles to Co metal and possibly partial reduction of highly dispersed Co_3O_4 to CoO. The reduction of RuO_2 to Ru^0 which usually takes place at lower temperatures than the reduction of Co_3O_4 [32,33] did not exhibit a separate peak; that peak probably overlapped the first reduction peak of Co_3O_4. The second peak located at ca. 250–360 °C is assigned to the reduction of CoO (possibly) and Co species that are highly dispersed and strongly interacting with the SiO_2 support. As Co loading increased, the reduction peaks in TPR of $CoRu/SiO_2$ shifted to higher temperatures. However, the presence of Ru as a promoter resulted in lower reduction temperatures compared to non-promoted Co/SiO_2 [10] as a result of hydrogen spillover.

The M1-supported CoRu catalysts exhibited quite different TPR profiles from the SiO_2-supported ones. More than two major reduction peaks were observed and significant reduction peaks were in evidence above 600 °C for ≥8 wt.% Co, suggesting that Co exhibited a stronger interaction with MCM-41 than with SiO_2.

The M2-supported CoRu catalysts exhibited quite similar TPR profiles to the SiO_2-supported ones with two major reduction peaks being observed. For the same Co loading, the first peaks were located at essentially the same temperature as $CoRu/SiO_2$. The second peaks for CoRu/M2, however, were located at much higher temperatures, especially for higher Co loading catalysts.

The reducibilities of the catalysts during TPR 30–800 °C and during TPR 30–400 °C are reported in Table 2. The reducibilities of all the catalysts during

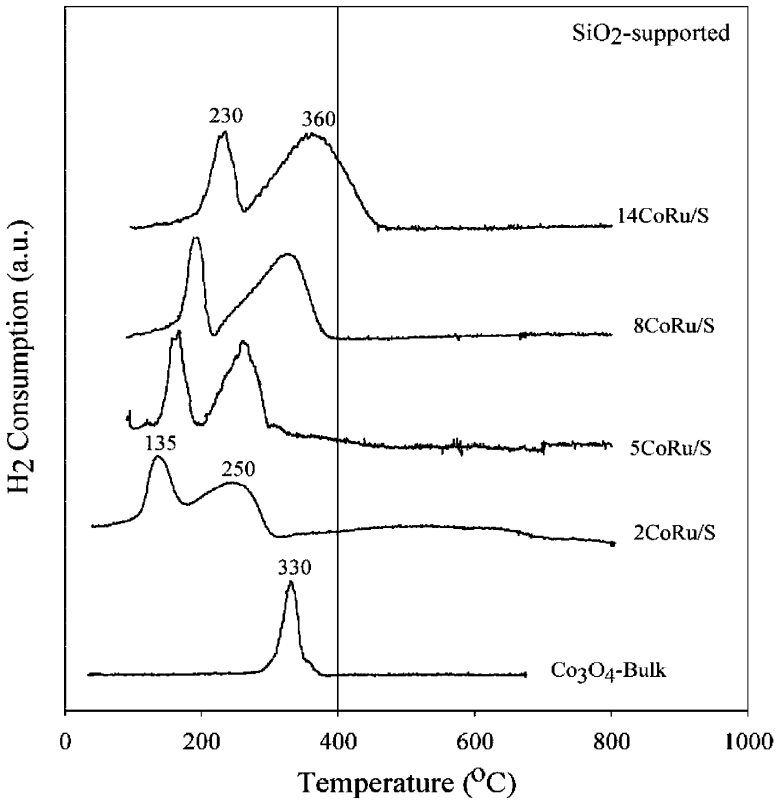

Fig. 8. TPR profiles of bulk Co_3O_4 and the $CoRu/SiO_2$ catalysts with different Co loadings.

TPR 30–800 °C were not significantly different, ranging from 60 to 70%. Any Co not reducible during TPR is identified as "non-reducible" Co silicate [5,34]. The reducibilities during TPR 30–400 °C, however, for the M1- and M2-supported catalysts, especially for high Co loadings, were much lower than those of the SiO_2-supported ones. The reducibility during TPR 30–400 °C is especially important because it has been found to correlate with the reducibility of the catalysts during the optimum standard reduction procedure (reduction at 350 °C in flowing H_2 for 10 h after ramping to that temperature at 1 °C/min) [26]. This reducibility is related to the amount of active Co^0 available for catalyzing FTS after standard reduction.

3.4. H_2 chemisorption

The total hydrogen uptakes, the percentages of cobalt dispersion, and the average diameters of reduced Co^0 particles (d_r) are reported in Table 2. The total hydrogen uptake was used to calculate cobalt metal particle size and dispersion since it has been reported to more accurately represent Co metal dispersion on silica [29]. Ru promotion has been reported previously to result in an increase in dispersion of Co on SiO_2 [10]. For the SiO_2-supported catalysts, the higher is the Co loading, the greater is the amount of H_2 chemisorbed. The result was similar for the M2-supported catalysts. However, for the M1-supported ones, the increase in the amount of H_2 chemisorbed with Co loading was minimal for Co loadings $\geq$ 5 wt.%, apparently due in part to a decrease in reducibility of the catalysts at the standard reduction condition (350 °C) and also possibly to a pore blocking effect. Average particle size for reduced Co (d_r) was calculated to be in the range of 3.9–7.6 nm. These average Co^0 particle sizes for the reduced catalysts calculated based on H_2 chemisorp-

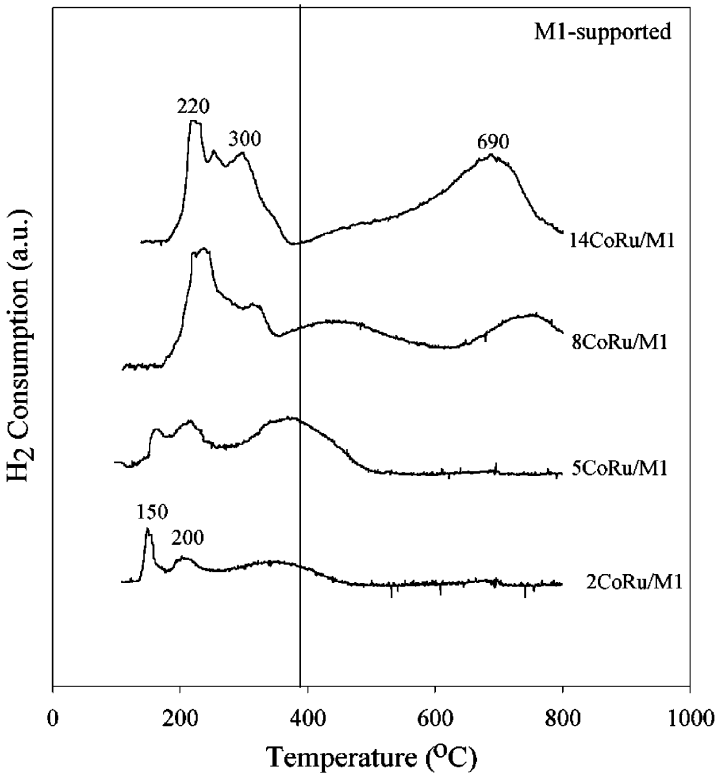

Fig. 9. TPR profiles of the CoRu/M1 catalysts with different Co loadings.

tion are not identical of course to the calculated Co_3O_4 particle sizes for the calcined catalysts obtained by XRD, since only a portion of Co was reducible. The M1- and M2-supported catalysts with low Co loadings appeared to have smaller average Co^0 particle sizes compared to those of the SiO_2-supported ones, resulting in their relatively high Co dispersions. However, 14CoRu/M1 had the lowest Co dispersion due to its significantly lower reducibility during standard reduction. The average Co^0 particle size on M1 for all Co loadings was calculated to be larger than the average pore diameter of M1. Part of this was probably due to larger Co^0 particles being on the external surface of the M1 granules. However, a contribution to this may have also been particles occluded in the pores. Pore blockages probably occurred, especially when a large amount of Co was impregnated, as evidenced by the decrease seen in pore volume with Co loading for both CoRu/M1 and CoRu/M2.

3.5. SEM and EDX

SEM and EDX were carried out for all the catalysts. Typical SEM micrographs of cross-sectioned catalyst granules of 8CoRu/S, 8CoRu/M1, and 8CoRu/M2 with locations of EDX analysis are shown in Figs. 11–13, respectively. The corresponding elemental distributions are reported in Table 3. The term

Table 3
EDX results[a]

Spectrum	Co (wt.%)		
	8CoRu/S	8CoRu/M1	8CoRu/M2
1	6.6	17.2	7.3
2	6.0	4.5	4.7
3	7.4	4.1	5.7
4	6.8	5.6	7.7
5	8.4	10.1	8.9

[a] Error of measurements was ±5%.

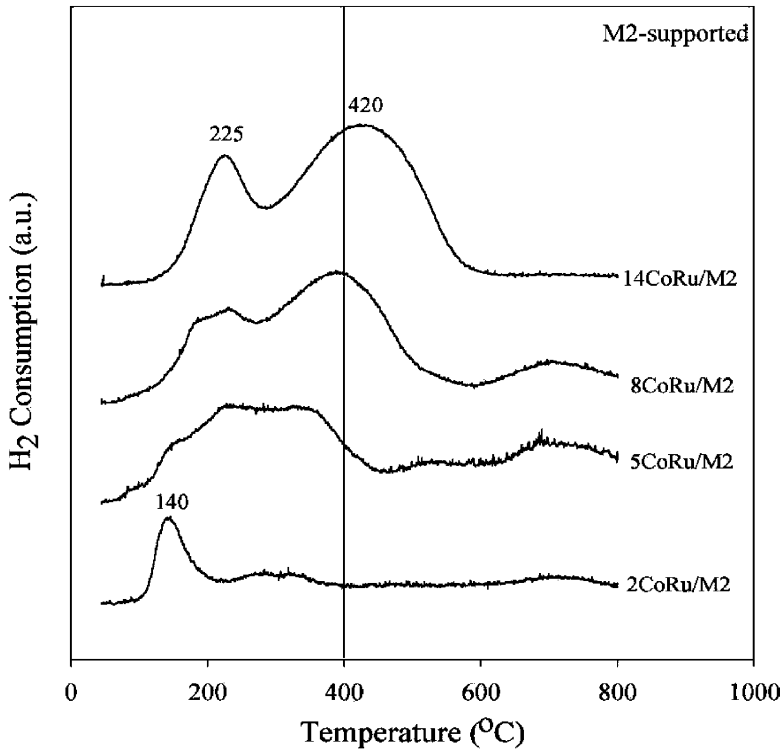

Fig. 10. TPR profiles of the CoRu/M2 catalysts with different Co loadings.

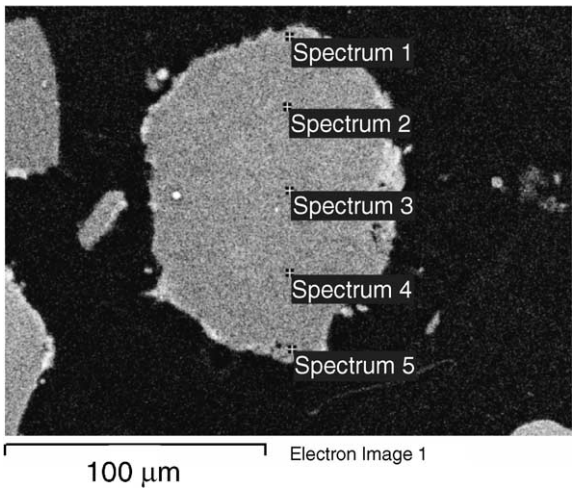

Fig. 11. SEM micrograph of 8CoRu/S with locations of EDX analysis.

"granule" here refers to a catalyst particle composed of Co, Ru, and silica (SiO_2 or MCM-41). In all the SEM figures, the white or light spots on the catalyst granules represent a high concentration of cobalt and its compounds while the darker areas of the granules indicate the support with minimal/no cobalt present. The dark background is due to the carbon tape used for holding the catalyst samples. It was observed from both SEM and EDX that the concentration of cobalt was similar at different points of interest on the cross-sectioned granules of the 8CoRu/S and 8CoRu/M2 catalysts, whereas, for 8CoRu/M1, the concentration of cobalt was higher at the edges of the catalyst granules than in the interior. This distribution difference was also seen for 14CoRu/M1, suggesting that for the smaller pore MCM-41 (M1), using incipient wetness impregnation resulted in cobalt not being uniformly deposited throughout the pores of the MCM-41 but concentrated more towards the external surface of the catalyst granules, especially for high Co loadings. However, for the lowest Co loading

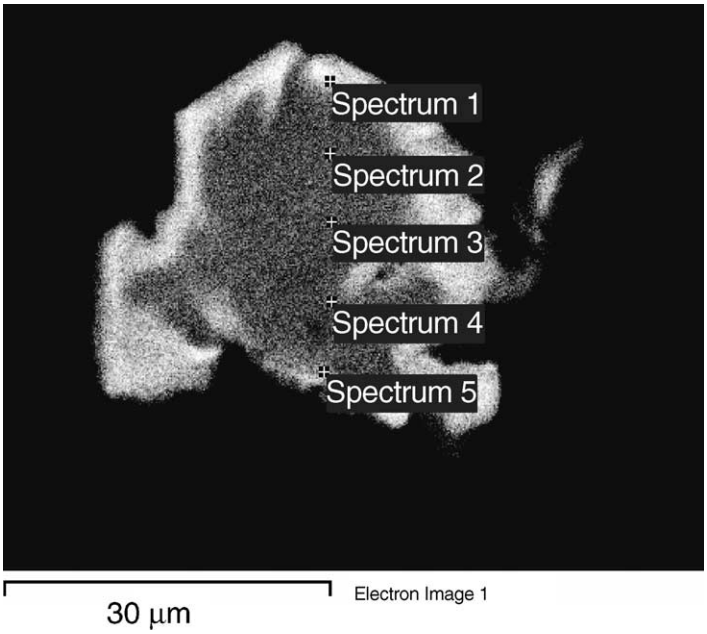

Fig. 12. SEM micrograph of 8CoRu/M1 with locations of EDX analysis.

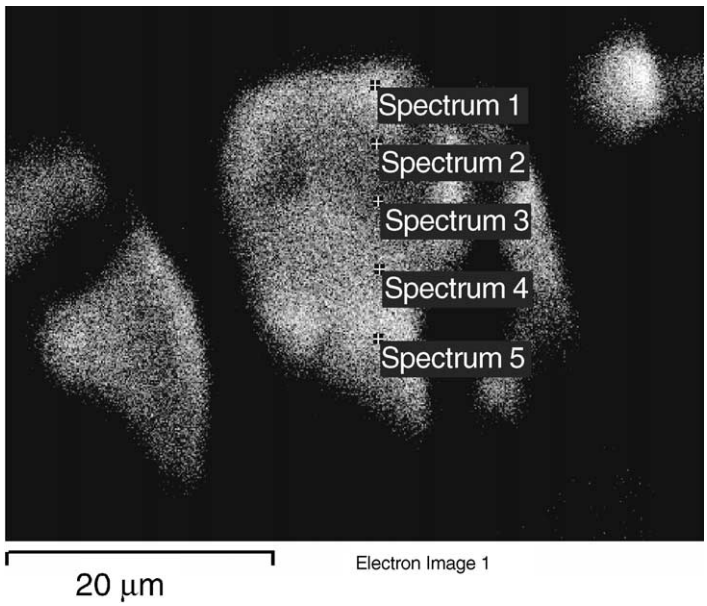

Fig. 13. SEM micrograph of 8CoRu/M2 with locations of EDX analysis.

Table 4
FTS steady-state results[a]

Catalysts	CO conversion (%)	Total rate (g CH_2/g cat/h)	TOF[b] ($\times 10^3$ s^{-1})	Selectivity (wt.%)				Chain growth probability (α) (C_5–C_{15})	E_A (kJ/mol)
				C_1	C_2–C_4	C_5–C_{12}	C_{13+}		
2CoRu/S	3.4	0.12	55.6	20.4	48.4	30.7	0.6	0.56	95
5CoRu/S	7.5	0.23	63.9	19.8	47.0	32.4	0.8	0.56	–
8CoRu/S	4.4	0.25	38.3	19.4	46.0	34.2	0.5	0.58	–
14CoRu/S	5.8	0.33	35.4	18.8	44.5	36.3	0.4	0.60	–
2CoRu/M1	4.8	0.16	72.5	20.0	47.5	32.1	0.4	0.56	88
5CoRu/M1	6.1	0.21	42.4	19.9	47.2	32.3	0.6	0.57	–
8CoRu/M1	5.1	0.29	52.8	19.6	46.5	33.3	0.3	0.60	–
14CoRu/M1	7.7	0.44	74.4	19.4	46.2	33.8	0.6	0.61	–
2CoRu/M2	4.7	0.16	75.9	20.1	47.8	31.9	0.3	0.53	102
5CoRu/M2	7.2	0.24	56.1	19.9	47.3	32.4	0.2	0.54	–
8CoRu/M2	4.6	0.26	47.0	20.1	47.8	31.7	0.2	0.56	–
14CoRu/M2	7.2	0.40	34.2	19.9	47.3	32.7	0.2	0.57	–

[a] The reaction conditions were 220 °C and 1 atm, $H_2/CO = 2$. Error of measurement was ±5%.
[b] Based on total H_2 chemisorption.

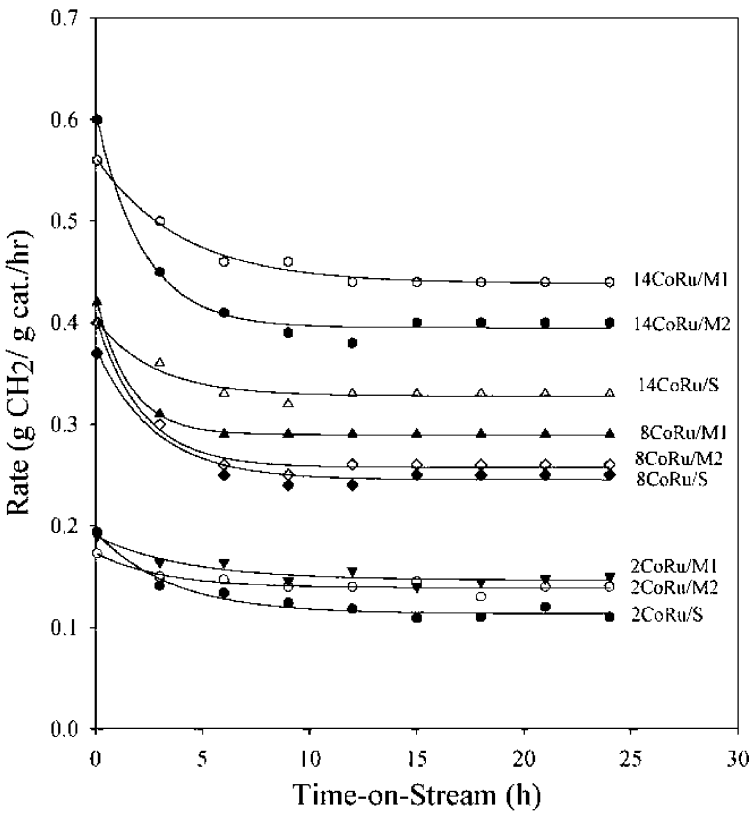

Fig. 14. Reaction rate at 220 °C vs. time-on-stream.

(2 wt.% Co) the distribution of cobalt was found to be uniform on all types of supports.

3.6. Fischer–Tropsch synthesis

FTS results are summarized in Table 4. The MCM-41 supported CoRu catalysts were found to have somewhat higher FTS activities (on a gram catalysts basis) than the SiO_2-supported ones with similar Co loadings. The variation of FTS activity as a function of time-on-stream for different CoRu catalysts (with 2, 8, and 14 wt.% Co) is shown in Fig. 14. The results (i.e., decrease in rate with TOS) were similar for the 5 wt.% Co catalysts (not shown in Fig. 14). In general, steady-state reaction was reached after 6 h on stream. For 2CoRu/M1 and 2CoRu/M2, the rate at steady-state was ca. 80% of the initial rate, while for 2CoRu/S, it was ca. 65%.

The steady-state TOF for FTS was fairly constant among the different CoRu catalysts used in this study (in the range of 0.034–0.076 s^{-1}). FTS is usually considered to be a structure-insensitive reaction and as such would not be expected to exhibit significant differences in TOF for different Co loadings and dispersion, barring major metal–support interactions capable of affecting Co^0 activity. While the TOF of CoRu/S and of CoRu/M2 decreased with Co loading, that of CoRu/M1 did not show any obvious trend.

Transport limitations due to the restricted pore structure of the MCM-41 did not appear to be a factor. The catalyst most likely to be impacted by this limitation because of its small pore size and distribution of Co, 2CoRu/M1, had an apparent activation energy of 88 kJ/mol, typical for FTS and close to that for 2CoRu/S (95 kJ/mol). Within experimental error, there was no significant difference in chain growth probability ($\alpha = 0.5$–0.6) for all the catalysts. Therefore, MCM-41-supported CoRu catalysts did not exhibit any shape-selective behavior or diffusional effects on selectivity at the reaction conditions used.

4. Discussion

Using MCM-41 as a metal support resulted in catalysts with much higher BET surface areas even at high Co loadings. The decrease in surface area, pore volume, and average pore diameter of MCM-41 as Co loading increased suggests that Co particles were deposited in the pores of the MCM-41 and this was confirmed by EDX. It is also possible that some loss of surface area and pore volume was partially due to pore blocking, especially when MCM-41 with smaller diameter pores (M1) was used as the support. Although, the ordered structure of MCM-41 was not detectable when $\geq$2 wt.% Co was loaded, the XRD results of the catalysts after removal of the metals by acid leaching indicated that the MCM-41 ordered structure was not destroyed by the preparation of supported CoRu catalysts. The disappearance of the XRD pattern due to MCM-41 for the catalysts with Co loading $\geq$ 2 wt.% was probably due to the greater diffraction ability of the metal particles, as has been reported before [35]. Based on the XRD results at low 2θ angles, it would appear that the large pore MCM-41 (M2) is more amorphous than M1. The only difference from amorphous silica was that M2 had a narrow pore size distribution with uniform pore diameters around 7 nm.

It is known that reduction of cobalt in the oxide form, Co_3O_4 or Co_2O_3, to Co^0 involves a two-step reduction: first reduction of Co_3O_4 or Co_2O_3 to CoO and then the subsequent reduction of CoO to Co^0 [25,26]. The two reduction steps may not always be observed as separate peaks in TPR [29,36–38], as seen in Fig. 7 for the reduction of bulk Co_3O_4 powder. However, a separation of the two reduction steps has often been found for supported cobalt catalysts due to interactions between Co_3O_4 and support materials such as silica or alumina. A wide range of variables including Co particle size [36], support interaction [37,40], and reduction gas composition [41] have an influence on the reduction behavior of cobalt catalysts resulting in the observation of different locations of the TPR peaks. The effects of particle size and support interaction, however, can superimpose on each other. Thus, while a decrease in metal oxide particle size can result in faster reduction due to a greater surface area/volume ratio, smaller particles may interact more with the support slowing reduction. A number of publications have appeared dealing with the study of the interaction between metal and support on silica- and alumina-supported cobalt catalysts [5,33,34]. Co–support species such as Co “silicates” and Co “aluminates” have been identified. Water vapor produced during metal reduction has been reported to facilitate the formation of these Co–support species

resulting in a decrease in the degree of reduction of the cobalt [5,26,34,37]. This probably explains why, when MCM-41 was used as the support, lower reducibilities of the catalysts during standard reduction (as measured by TPR 30–400 °C) resulted. Due to the restricted pore structure of the MCM-41, higher partial pressures of water vapor could develop in the pores, especially for high Co loadings where larger amounts of water vapor would be produced. The water vapor effect would be expected to be more pronounced for the M1-supported catalysts than the M2-supported ones because of the much smaller pore diameter of the M1. Thus, it is not surprising that Co in CoRu/M1 was harder to reduce (as shown by higher temperature TPR peaks).

The results from H_2 chemisorption show that both M1- and M2-supported CoRu catalysts had comparable Co dispersions to the SiO_2-supported ones with similar Co loadings. Although MCM-41 has much higher BET surface areas than amorphous silica, a higher metal dispersion was not observed due to the decrease in the extent of Co reduction able to be achieved during standard reduction of the MCM-41 supported catalysts. The average Co^0 metal particle size determined from H_2 chemisorption was also quite similar for the same Co loading on different supports and in general increased with increasing Co loading. The average Co^0 metal particle size for M1-supported catalysts (3.9–7.6 nm) was, however, found to be larger than the average pore diameter of M1 (3 nm). If this was the case, therefore, most Co particles would exist only on the external surface of the MCM-41, not inside the pores. Nevertheless, overestimation of Co metal particle is possible due to (a) partial blockage of hydrogen chemisorption as a result of agglomeration of metal particles in the pores that render some portions of the metal particles inaccessible to H_2 adsorption [42] and (b) localized destruction of the well-defined pore structure forming cracks and holes where larger metal particle could form [43]. There is no evidence of H_2 chemisorption suppression since the TOF results for FTS on the three series of the catalysts are quite similar. Thus, it is most likely that some of the Co metal particles existed as large particles on the external surface of the MCM-41 and some existed as very small particles inside the MCM-41 pores where H_2 chemisorption may have been partially blocked, resulting in the larger average particle diameters being determined.

SEM and EDX provided additional information about the elemental distribution of the three types of supported CoRu catalysts. For low Co loading (2 wt.%), the distribution of cobalt was found to be uniform throughout the catalyst granules for all types of support. For M2- and SiO_2-supported catalysts the uniform distribution of cobalt was observed for all Co loadings studied (2–14 wt.%). However, for M1-supported catalysts, as Co loading increased, cobalt was found to be concentrated more towards the outer surface of the catalyst granules and less evenly distributed. This suggests that, if uniform distribution of Co metal is desired at higher Co loadings on MCM-41 having small pores, multiple impregnations of the Co precursor are required. A preparation technique for highly dispersed Co on MCM-41 can also be found in Ref. [44].

Because of uniform Co distribution throughout the granules of 2CoRu/M1, initially reaction would be expected to occur throughout the catalyst pores. If the pores became blocked during reaction so that most/all of the Co surfaces within pores became inaccessible for reaction, one would expect to have seen a significant loss of activity with TOS. This did not happen, as seen in Fig. 14. The degree of deactivation with TOS for 2CoRu/M1 was similar to that of 2CoRu/S. At steady-state, the apparent activation energy also did not indicate any diffusion limitations. For catalysts with higher Co loadings, Co was concentrated more towards the external surface of the catalyst granules. Certainly, reaction did take place more towards the external surface of the MCM-41 granules on those catalysts due to the distribution of the Co. However, there is no evidence for those catalysts either that reaction on the Co particles inside the pore was blocked. The TOF values for FTS did not vary significantly with support or metal loading. There was an absence of any pore size effect on the product rate or selectivity probably due to pores being sufficiently large for the reaction to easily proceed at 1 atm and 220 °C, the reaction conditions used.

5. Conclusion

Compared to $CoRu/SiO_2$, CoRu/MCM-41 had much higher BET surface areas, even at high Co loadings. The ordered structure of MCM-41 was pre-

served after the preparation of the CoRu catalysts as confirmed by the XRD results of the catalysts after removal of the Co and Ru metals by acid leaching. CoRu/MCM-41 manifested lower reducibilities during standard reduction than CoRu/SiO_2. The Co–support interaction became stronger when MCM-41 was used as a support as shown by higher temperature TPR peaks, especially for the smaller pore MCM-41 with high Co loadings. Its restricted mesopore structure probably impedes the diffusion of the water out of the pores during reduction, facilitating the formation of more difficult to reduced Co–support species. CoRu/MCM-41 had comparable percent Co dispersion to CoRu/SiO_2 for similar Co loadings. The results from N_2 physisorption, H_2 chemisorption, and EDX suggest that pore blockages probably occurred when a large amount of Co was impregnated into the small pore MCM-41 resulting in non-uniform distribution of cobalt. This suggests that, if uniform distribution of Co metal is desired at higher Co loadings on MCM-41 having small pores, multiple impregnations of the Co precursor are required. There was an absence of any pore size effect on the reaction rate or selectivity probably due to the pores being sufficiently large for the reaction to easily proceed at 1 atm and 220 °C. The results of this study clearly demonstrate that active Co FTS catalysts can be prepared using MCM-41 as a support. Given flexibility of preparing MCM-41 with uniform small–medium pores and with a variety of metal substitutions in the SiO_2 framework, interesting possibilities exist for the preparation of a wide variety of new Co catalysts having unique and tailored properties.

Acknowledgements

The authors would like to acknowledge the financial support of JP by the Royal Thai Government.

References

[1] R.S. Young, Cobalt: Its Chemistry, Metallurgy and Uses, American Chemical Society, Reinhold, NY, 1960.
[2] R.C. Reuel, C.H. Bartholomew, J. Catal. 85 (1984) 78.
[3] S. Sun, N. Tsubaki, K. Fujimoto, Appl. Catal. A 202 (2000) 121.
[4] G.J. Haddad, J.G. Goodwin Jr., J. Catal. 157 (1995) 25.
[5] L.B. Backman, A. Rautiainen, A.O.I. Krause, M. Lindblad, Catal. Today 43 (1998) 11.
[6] C. Sellmer, S. Decker, N. Kruse, Catal. Lett. 52 (1998) 131.
[7] S. Ali, B. Chen, J.G. Goodwin Jr., J. Catal. 157 (1995) 35.
[8] J. van de Loosdrecht, M. van der Haar, A.M. van der Krann, J.W. Geus, Appl. Catal. A 150 (1997) 365.
[9] A.R. Belambe, R. Oukaci, J.G. Goodwin Jr., J. Catal. 166 (1997) 8.
[10] A. Kogelbauer, J.G. Goodwin Jr., R. Oukaci, J. Catal. 160 (1996) 125.
[11] D. Schanke, A.M. Hilmen, E. Bergene, K. Kinnari, E. Rytten, E. Adnanes, A. Holmen, Catal. Lett. 34 (1995) 269.
[12] B. Viswanathan, R.J. Gopalakrishnan, J. Catal. 99 (1986) 342.
[13] J.H.A. Martens, H.F.J. van't Blik, R. Prins, J. Catal. 97 (1986) 200.
[14] J. Li, N.J. Coville, Appl. Catal. A 181 (1999) 201.
[15] F.B. Naronha, M. Schmal, C.J. Nicot, B. Morawek, R. Frety, J. Catal. 168 (1997) 42.
[16] S. Bessell, Appl. Catal. A 126 (1995) 235.
[17] D.J. Koh, S.C. Jong, Y.G. Kim, Ind. Eng. Chem. Res. 34 (1995) 1969.
[18] S. Bessell, Appl. Catal. A 96 (1990) 253.
[19] A. Corma, A. Martinez, V. Soria, J. Catal. 169 (1997) 480.
[20] C. Song, K.M. Reddy, Appl. Catal. A 176 (1999) 1.
[21] F. Schuth, A. Wingen, J. Sauer, Micropor. Mesopor. Mater. 44–45 (2001) 465.
[22] M. Kruk, M. Jaroniec, A. Sayari, Micropor. Mesopor. Mater. 35–36 (2000) 545.
[23] H.P. Klug, L.E. Alexander, X-ray Diffraction Procedures for Polycrystalline, Amorphous Materials, 2nd ed., Wiley, New York, 1974.
[24] R.B. Anderson, The Fischer–Tropsch Synthesis, Academic Press, Orlando, 1984.
[25] D. Schanke, S. Vada, E.A. Blekkan, A. Hilmen, A. Hoff, A. Holmen, J. Catal. 156 (1995) 85.
[26] Y. Zhang, D. Wei, S. Hammache, J.G. Goodwin Jr., J. Catal. 188 (1999) 281.
[27] R.C. Reuel, C.H. Bartholomew, J. Catal. 85 (1984) 63.
[28] Y. Okamoto, K. Nagata, T. Adachi, T. Imanaka, K. Inamura, T. Takyu, J. Phys. Chem. 95 (1991) 310.
[29] A. Lapidus, A. Krylova, V. Kazanskii, Z. Borovkov, J. Ratnousky, A. Zukal, M.C. Jan, Appl. Catal. A 73 (1991) 65.
[30] B. Ernst, S. Libs, P. Chaumette, A. Kiennemann, Appl. Catal. A 186 (1999) 145.
[31] E. van Steen, G.S. Sewell, R.A. Makhothe, C. Micklethwaite, H. Manstein, M. de Lange, C.T. O'Connor, J. Catal. 162 (1996) 220.
[32] N.W. Hurst, S.J. Gentry, A. Jones, B.D. McNicol, Catal. Rev. Sci. Eng. 24 (2) (1982) 233.
[33] P. Betancourt, A. Rives, R. Hubaut, C.E. Scott, J. Goldwasser, Appl. Catal. A 170 (1998) 307.
[34] A. Kogelbauer, J.C. Webber, J.G. Goodwin Jr., Catal. Lett. 34 (1995) 259.
[35] B. Marler, U. Oberhagemann, S. Vartmann, H. Gies, Micropor. Mater. 6 (1996) 375.
[36] P. Arnoldy, J.A. Moulijin, J. Catal. 93 (1985) 38.
[37] A.M. Hilmen, D. Schanke, A. Holmen, Catal. Lett. 38 (1996) 143.

[38] W. Wang, Y. Chen, Appl. Catal. A 77 (1991) 223.
[39] S.W. Ho, M. Houalla, D.M. Hercules, J. Phys. Chem. 94 (1990) 6396.
[40] H.F.J. van't Blik, R. Prins, J. Catal. 97 (1986) 188.
[41] J. Li, L. Xu, R. Keogh, B. Davis, Catal. Lett. 70 (2000) 127.
[42] J.J. Verdonck, P.A. Jacobs, M. Genet, G. Poncelet, J. Chem. Soc., Faraday Trans. 76 (1980) 403.
[43] B.L. Gustafson, J.H. Lunsford, J. Catal. 74 (1982) 393.
[44] A. Jentys, N.H. Pham, H. Vinek, M. Englisch, J.A. Lercher, Mircropor. Mater. 6 (1996) 13.